

Effects of Z_b states and bottom meson loops on $\Upsilon(4S) \rightarrow \Upsilon(1S, 2S)\pi^+\pi^-$ transitions

Yun-Hua Chen,¹ Martin Cleven,² Johanna T. Daub,¹ Feng-Kun Guo,^{3,4} Christoph Hanhart,⁵ Bastian Kubis,¹ Ulf-G. Meißner,^{1,5} and Bing-Song Zou^{3,4}

¹*Helmholtz-Institut für Strahlen- und Kernphysik (Theorie) and Bethe Center for Theoretical Physics, Universität Bonn, 53115 Bonn, Germany*

²*Departament de Física Quàntica i Astrofísica Universitat de Barcelona, 08028 Barcelona, Spain*

³*CAS Key Laboratory of Theoretical Physics, Institute of Theoretical Physics, Chinese Academy of Sciences, Beijing 100190, China*

⁴*School of Physical Sciences, University of Chinese Academy of Sciences, Beijing 100049, China*

⁵*Institut für Kernphysik, Institute for Advanced Simulation, and Jülich Center for Hadron Physics, Forschungszentrum Jülich, 52425 Jülich, Germany*

(Received 4 November 2016; published 21 February 2017)

We study the dipion transitions $\Upsilon(4S) \rightarrow \Upsilon(nS)\pi^+\pi^-$ ($n = 1, 2$). In particular, we consider the effects of the two intermediate bottomoniumlike exotic states $Z_b(10610)$ and $Z_b(10650)$ as well as bottom meson loops. The strong pion-pion final-state interactions, especially including channel coupling to $K\bar{K}$ in the S wave, are taken into account model independently by using dispersion theory. Based on a nonrelativistic effective field theory we find that the contribution from the bottom meson loops is comparable to those from the chiral contact terms and the Z_b -exchange terms. For the $\Upsilon(4S) \rightarrow \Upsilon(2S)\pi^+\pi^-$ decay, the result shows that including the effects of the Z_b exchange and the bottom meson loops can naturally reproduce the two-hump behavior of the $\pi\pi$ mass spectra. Future angular distribution data are decisive for the identification of different production mechanisms. For the $\Upsilon(4S) \rightarrow \Upsilon(1S)\pi^+\pi^-$ decay, we show that there is a narrow dip around 1 GeV in the $\pi\pi$ invariant mass distribution, caused by the final-state interactions. The distribution is clearly different from that in similar transitions from lower Υ states, and needs to be verified by future data with high statistics. Also we predict the decay width and the dikaon mass distribution of the $\Upsilon(4S) \rightarrow \Upsilon(1S)K^+K^-$ process.

DOI: [10.1103/PhysRevD.95.034022](https://doi.org/10.1103/PhysRevD.95.034022)

I. INTRODUCTION

The processes of dipion emission of the bottomonia $\Upsilon(mS) \rightarrow \Upsilon(nS)\pi\pi$ are important for understanding the heavy-quarkonium dynamics and low-energy QCD. Because the bottomonia are expected to be nonrelativistic and compact, the method of the QCD multipole expansion [1–4] is often used to study these transitions, where the pions emitted come from the hadronization of soft gluons. Though successful in describing many $\Upsilon(mS) \rightarrow \Upsilon(nS)\pi\pi$ processes, a well-known anomaly about the method of the QCD multipole expansion is that it cannot reproduce the two-hump behavior in the experimental $\pi\pi$ invariant mass spectra of the decays $\Upsilon(3S) \rightarrow \Upsilon(1S)\pi\pi$ and $\Upsilon(4S) \rightarrow \Upsilon(2S)\pi^+\pi^-$ [5–7]. In a previous study [8], we found that by including the effects of the two bottomoniumlike exotic states $Z_b(10610)$ and $Z_b(10650)$ discovered by the Belle Collaboration [9,10] as well as the $\pi\pi$ final-state interaction (FSI), the anomaly of the $\Upsilon(3S) \rightarrow \Upsilon(1S)\pi\pi$ process can be naturally explained. Such an analysis is a modern version of the much earlier studies in Refs. [11,12], where an isovector $b\bar{b}q\bar{q}$ state was considered. Although the direct decay of Z_b into $\Upsilon(4S)\pi$ is kinematically impossible, it may be illuminating to analyze the effect of the Z_b -exchange mechanism in the $\Upsilon(4S) \rightarrow \Upsilon(1S, 2S)\pi^+\pi^-$

processes, which is performed in this study. In this context it is important to note that improved data on $\Upsilon(nS)$ decays are to be expected from Belle-II that will start operation soon—for a detailed discussion of prospects for various decays relevant for this study we refer to Ref. [13].

The $\Upsilon(4S)$ meson is above the $B\bar{B}$ threshold and decays predominantly to $B\bar{B}$, so loop effects with intermediate bottom mesons may play an important role in $\Upsilon(4S) \rightarrow \Upsilon(nS)\pi\pi$ ($n = 1, 2$). Also, the inclusion of the loops introduces nonanalyticities arising from the $B\bar{B}$ threshold needed to be taken into account in dispersion theory, which is discussed later. Because the bottomonia are close to the open-bottom meson production threshold, the velocity of the intermediate bottom mesons is small and can be treated as an expansion parameter to build power-counting rules in a nonrelativistic effective field theory (NREFT) [14–16]. Within the NREFT scheme, we calculate the dominant box diagrams in the dipion emissions of $\Upsilon(4S)$, and find that their contribution is comparable in size to the chiral contact terms and the Z_b -exchange graphs.

In the $\Upsilon(4S) \rightarrow \Upsilon(1S)\pi\pi$ process, the dipion invariant mass reaches above the $K\bar{K}$ threshold, so the coupled-channel FSI in the S wave is strong and needs to be taken into account. Based on analyticity and unitarity, dispersion

theory can achieve this in a model-independent way. In this study, we use dispersion theory in the form of modified Omnès solutions, in which the left-hand-cut contribution is approximated by the sum of the Z_b -exchange mechanism and the bottom meson loops. At low energies, the amplitude should agree with the leading chiral results, so the subtraction functions can be determined by matching to chiral contact terms. For the leading contact couplings of two S -wave bottomonia to an even number of light pseudoscalar mesons, we adopt the Lagrangian given in Ref. [17], constructed in the spirit of the chiral and the heavy-quark nonrelativistic expansions.

This paper is organized as follows. In Sec. II, we present the theoretical framework and elaborate on the calculation of the amplitudes as well as the dispersive treatment of the FSI. In Sec. III, we fit the experimental data of the $\pi\pi$ invariant mass distribution to determine the coupling constants, and discuss the contributions of different mechanisms. A summary is given in Sec. IV.

II. THEORETICAL FRAMEWORK

A. Lagrangians

Because in the heavy-quark limit the spin of the heavy quarks decouples, it is convenient to introduce the heavy quarkonia and heavy hadrons in terms of spin multiplets. One has $J \equiv \Upsilon \cdot \boldsymbol{\sigma} + \eta_b$, where Υ and η_b annihilate the Υ and η_b states, respectively, and $\boldsymbol{\sigma}$ contains the Pauli matrices [18]. The bottom mesons are collected in $H_a = \mathbf{V}_a \cdot \boldsymbol{\sigma} + P_a$ with $P_a(V_a) = (B^{(*)-}, \bar{B}^{(*)0}, \bar{B}_s^{(*)0})$, and $\bar{H}_a = -\bar{\mathbf{V}}_a \cdot \boldsymbol{\sigma} + \bar{P}_a$ with $\bar{P}_a(\bar{V}_a) = (B^{(*)+}, B^{(*)0}, B_s^{(*)0})$ [19].

The effective Lagrangian for the contact $\Upsilon\Upsilon'\pi\pi$ and $\Upsilon\Upsilon'K\bar{K}$ coupling, at the lowest order in the chiral as well as the heavy-quark expansion, reads [8,17]

$$\mathcal{L}_{\Upsilon\Upsilon'\Phi\Phi} = \frac{c_1}{2} \langle J^\dagger J' \rangle \langle u_\mu u^\mu \rangle + \frac{c_2}{2} \langle J^\dagger J' \rangle \langle u_\mu u_\nu \rangle v^\mu v^\nu + \text{H.c.}, \quad (1)$$

where $v^\mu = (1, \mathbf{0})$ is the velocity of the heavy quark. The Goldstone bosons of the spontaneous breaking of chiral symmetry can be parametrized as

$$u_\mu = i(u^\dagger \partial_\mu u - u \partial_\mu u^\dagger), \quad u = \exp\left(\frac{i\Phi}{\sqrt{2}F}\right),$$

$$\Phi = \begin{pmatrix} \frac{1}{\sqrt{2}}\pi^0 + \frac{1}{\sqrt{6}}\eta_8 & \pi^+ & K^+ \\ \pi^- & -\frac{1}{\sqrt{2}}\pi^0 + \frac{1}{\sqrt{6}}\eta_8 & K^0 \\ K^- & \bar{K}^0 & -\frac{2}{\sqrt{6}}\eta_8 \end{pmatrix}, \quad (2)$$

where F is the pseudo-Goldstone boson decay constant, and we use $F_\pi = 92.2$ MeV for the pions and $F_K = 113.0$ MeV for the kaons. The two operators in Eq. (1)

both scale as $\mathcal{O}(q_\pi^2)$ in the expansion in (soft) pion momenta q_π .

The leading Lagrangian for the $Z_b\Upsilon\pi$ interaction, which is needed in the calculation of the mechanism $\Upsilon(mS) \rightarrow Z_b\pi \rightarrow \Upsilon(nS)\pi\pi$, reads [18]¹

$$\mathcal{L}_{Z_b\Upsilon\pi} = \sum_{j=1,2} \sum_l C_{Z_b\Upsilon(lS)\pi} \Upsilon^i(lS) \langle Z_{bj}^\dagger u_\mu \rangle v^\mu + \text{H.c.}, \quad (3)$$

where Z_{b1} and Z_{b2} are used to refer to $Z_b(10610)$ and $Z_b(10650)$, respectively. The Z_b states are collected in the matrix as

$$Z_{bj}^i = \begin{pmatrix} \frac{1}{\sqrt{2}}Z_{bj}^{0i} & Z_{bj}^{+i} & 0 \\ Z_{bj}^{-i} & -\frac{1}{\sqrt{2}}Z_{bj}^{0i} & 0 \\ 0 & 0 & 0 \end{pmatrix}. \quad (4)$$

Note that since strange partners of the Z_b states, Z_{bs} , have not been observed, we set the corresponding matrix entries in Eq. (4) to 0.

To calculate the box diagrams, we need the Lagrangian for the coupling of the S -wave bottomonium fields to the bottom and antibottom mesons [14],

$$\mathcal{L}_{JHH} = \frac{ig_{JHH}}{2} \langle J^\dagger H_a \boldsymbol{\sigma} \cdot \vec{\partial} \bar{H}_a \rangle + \text{H.c.}, \quad (5)$$

where $A\vec{\partial}B \equiv A(\vec{\partial}B) - (\vec{\partial}A)B$. We also need the Lagrangian for the axial coupling of the Goldstone bosons to the bottom and antibottom mesons, which at leading order heavy-flavor chiral perturbation theory is given by [19–23]

$$\mathcal{L}_{HH\Phi} = \frac{g_\pi}{2} \langle \bar{H}_a^\dagger \boldsymbol{\sigma} \cdot \mathbf{u}_{ab} \bar{H}_b \rangle - \frac{g_\pi}{2} \langle H_a^\dagger H_b \boldsymbol{\sigma} \cdot \mathbf{u}_{ba} \rangle, \quad (6)$$

where $u^i = -\sqrt{2}\partial^i\Phi/F + \mathcal{O}(\Phi^3)$ corresponds to the three-vector components of u_μ as defined in Eq. (2). Here we use $g_\pi = 0.5$ from a recent lattice QCD calculation [24].²

B. Power counting of the loops

Since the $\Upsilon(4S)$ is above the $B\bar{B}$ threshold and decays predominantly into $B\bar{B}$ pairs, the loop mechanism with intermediate bottom mesons may play a significant role in the bottomonium transitions $\Upsilon(4S) \rightarrow \Upsilon(nS)\pi^+\pi^-$. In this section, we analyze the power counting of different kinds of loops, based on NREFT [14–16]. In NREFT, the expansion

¹Here we only include the terms relevant to the Υ coupling rather than the full spin multiplet defined before as $J = \Upsilon \cdot \boldsymbol{\sigma} + \eta_b$. In this way, we avoid the discussion of the internal spin structure of the Z_b states, which depends on specific models for Z_b and is not really settled yet.

²The precise value quoted in Ref. [24] is $g_\pi = 0.492 \pm 0.029$.

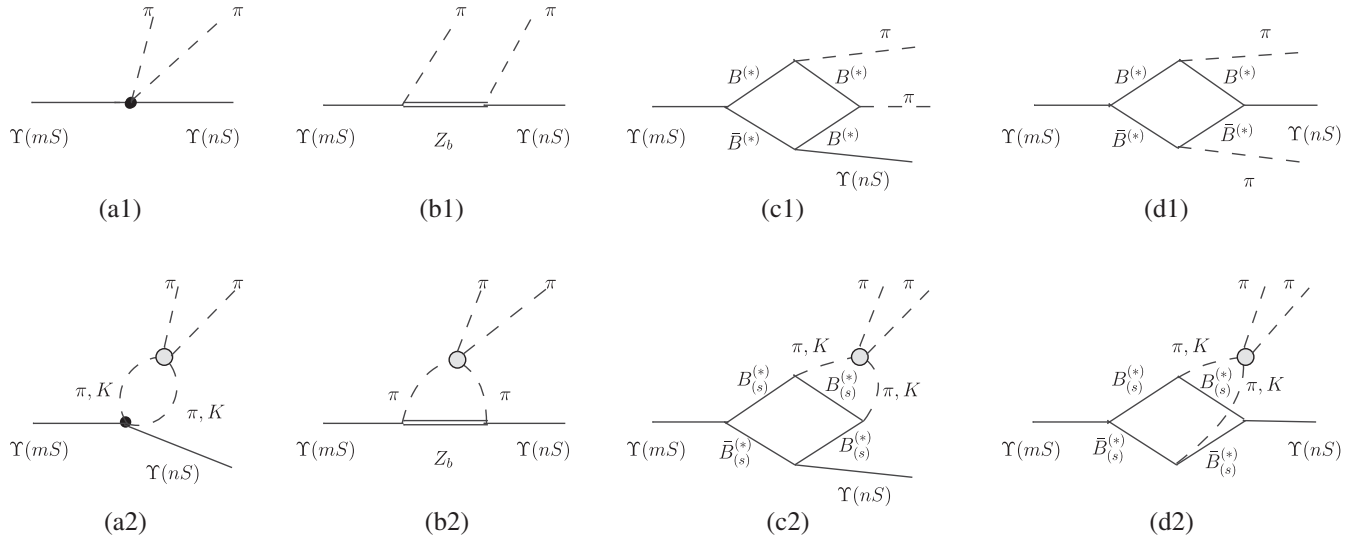


FIG. 1. Feynman diagrams considered for the $\Upsilon(mS) \rightarrow \Upsilon(nS)\pi\pi$ processes. The crossed diagrams of (b1), (c1), (b2), and (c2) are not shown explicitly. The gray blob denotes the final-state interaction.

parameter is the typical velocity of the intermediate heavy meson, namely, $\nu = \sqrt{|m_{\Upsilon(1S)} - m_{B^{(*)}} - m_{\bar{B}^{(*)}}|/m_{B^{(*)}}}$, and $\nu \ll 1$ since $\Upsilon(1S)$ are close to the $B^{(*)}\bar{B}^{(*)}$ thresholds. Each nonrelativistic propagator is counted as $1/\nu^2$, and the full integral measure $\int d^4l$ as ν^5 . More details of the power counting rules are elaborated in Ref. [15].

Without considering the FSI, there are five different kinds of loop contributions, namely, the box diagrams displayed in Figs. 1(c1) and 1(d1), and the triangle diagrams displayed in Figs. 2(a)–2(c). We analyze them one by one as follows:

- (i) Box diagrams, namely Figs. 1(c1) and 1(d1): As indicated in Eq. (6), the vertex for the axial coupling of the pion to the bottom mesons is proportional to the external momentum of the pion q_π . Both the vertices for the initial and final bottomonia are in a P wave, and the product of the two vertices can be counted as $\mathcal{O}(\nu^2)$, so the box diagrams are counted as $\nu^5 \nu^2 q_\pi^2 / \nu^8 = q_\pi^2 / \nu$. Note that these contributions thus have the same scaling in pion momenta as the leading $\Upsilon\Upsilon'\pi\pi$ contact terms from the Lagrangian Eq. (1), but are formally enhanced by $1/\nu$ in the nonrelativistic velocity parameter.

- (ii) Figure 2(a): The leading $B^{(*)}\bar{B}^{(*)}\pi\pi$ vertex comes from the covariant chiral derivative term $\langle H_a^\dagger(iD_0)_{ba}H_b \rangle = \langle H_a^\dagger(i\partial_0 - iV_0)_{ba}H_b \rangle$ [25,26], in which the pion pair produced by the vector current, $V^\mu = \frac{1}{2}(u^\dagger \partial^\mu u + u \partial^\mu u^\dagger)$, cannot form a positive-parity and C -parity state, so this leading vertex does not contribute to the $\Upsilon(mS) \rightarrow \Upsilon(nS)\pi\pi$ processes. Isoscalar, $PC = ++$ pion pairs only enter in the next order $\mathcal{O}(q_\pi^2)$ from point vertices. For the vertices of the initial and final bottomonia, both of them are in P waves, so the product of them can be counted as $\mathcal{O}(\nu^2)$. These diagrams hence count as $\nu^5 \nu^2 q_\pi^2 / \nu^6 = \nu q_\pi^2$, and are suppressed compared to the contact terms $\propto c_{1,2}$ by the factor ν .
- (iii) Figures 2(b) and 2(c): The leading $\Upsilon(1S)B^{(*)}\bar{B}^{(*)}\pi$ vertex given by $\langle J\bar{H}_a^\dagger H_b^\dagger \rangle u_{ab}^0$ [27] is proportional to the energy of the pion, $E_\pi \sim q_\pi$. In Fig. 2(b), the vertex for the initial bottomonium is in an S wave, and the vertex for the final bottomonium is in a P wave, so the loop momentum must contract with the external momentum q_π and hence the P -wave vertex scales as $\mathcal{O}(q_\pi)$. For this reason, Fig. 2(b) is counted as $\nu^5 q_\pi^3 / (\nu^6 m_B) = q_\pi^3 / (\nu m_B)$, where the factor m_B

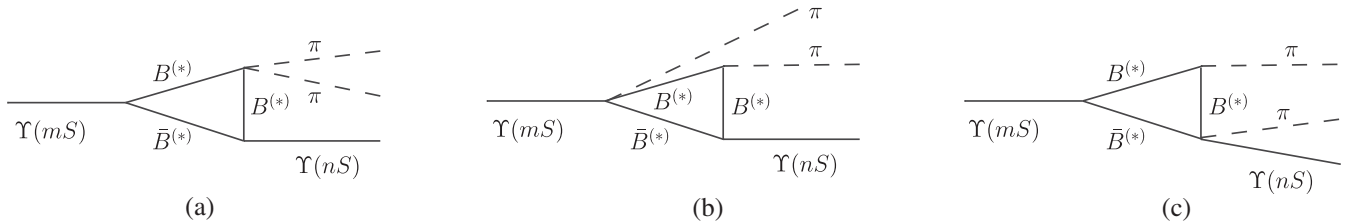


FIG. 2. Subleading contributions for $\Upsilon(mS) \rightarrow \Upsilon(nS)\pi\pi$ that are suppressed in comparison to the four-point functions in Fig. 1 and hence not considered in the calculations. The corresponding power counting arguments are given in the main text.

has been introduced to match the dimension with the scaling for cases 1 and 2. Analogous arguments hold for Fig. 2(c). This class of diagrams is therefore suppressed in the chiral expansion in pion momenta, compared to the $c_{1,2}$ terms.

We find thus that according to the power counting the box diagrams are dominant among the loop contributions, and the only ones not expected to be suppressed relative to the tree-level contact terms. We therefore only calculate those in the present study. Note that all (box and triangle) loop contributions discussed here are ultraviolet finite, and do not require the additional introduction of counterterms.

C. Tree-level amplitudes and box diagram calculation

First we define the Mandelstam variables in the decay process of $\Upsilon(mS)(p_a) \rightarrow \Upsilon(nS)(p_b)P(p_c)P(p_d)$,

$$s = (p_c + p_d)^2, \quad t_P = (p_a - p_c)^2, \quad u_P = (p_a - p_d)^2, \\ 3s_{0P} \equiv s + t_P + u_P = m_{\Upsilon(mS)}^2 + m_{\Upsilon(nS)}^2 + 2m_P^2, \quad (7)$$

where P denotes the pseudoscalar π or K , since we also need to take into account the virtual process $\Upsilon(mS)(p_a) \rightarrow \Upsilon(nS)(p_b)K(p_c)\bar{K}(p_d)$ in the coupled-channel FSI. t_P and u_P can be expressed in terms of s and the helicity angle θ according to

$$t_P = \frac{1}{2}[3s_{0P} - s + \kappa_P(s) \cos \theta], \\ u_P = \frac{1}{2}[3s_{0P} - s - \kappa_P(s) \cos \theta], \\ \kappa_P(s) \equiv \sigma_P \lambda^{1/2}(m_{\Upsilon(mS)}^2, m_{\Upsilon(nS)}^2, s), \\ \sigma_P \equiv \sqrt{1 - \frac{4m_P^2}{s}}, \quad (8)$$

where θ is defined as the angle between the initial $\Upsilon(mS)$ and the positive pseudoscalar in the rest frame of the PP system, and $\lambda(a, b, c) = a^2 + b^2 + c^2 - 2(ab + ac + bc)$. We define \mathbf{q} as the 3-momentum of the final bottomonium in the rest frame of the initial state with

$$|\mathbf{q}| = \frac{1}{2m_{\Upsilon(mS)}} \lambda^{1/2}(m_{\Upsilon(mS)}^2, m_{\Upsilon(nS)}^2, s). \quad (9)$$

The calculation of the tree amplitudes is very similar to our previous study of $\Upsilon(3S)$ decays [8], so here we just

quote the partial-wave-projected results. Parity and C -parity conservation require the pion pair to have even relative angular momentum l . We only consider the S -wave and D -wave components in this study, neglecting the effects of higher partial waves. For the S wave, the amplitudes of the chiral contact term and the Z_b -exchange term read

$$M_0^{\chi, P}(s) = -\frac{2}{F_P^2} \sqrt{m_{\Upsilon(mS)} m_{\Upsilon(nS)}} \left\{ c_1 (s - 2m_P^2) + \frac{c_2}{2} \left[s + \mathbf{q}^2 \left(1 - \frac{\sigma_P^2}{3} \right) \right] \right\}, \quad (10)$$

$$\hat{M}_0^{Z_b, \pi}(s) = -\frac{2\sqrt{m_{\Upsilon(mS)} m_{\Upsilon(nS)}}}{F_\pi^2 \kappa_\pi(s)} \\ \times \sum_{i=1,2} m_{Z_{bi}} C_{mn,i} \{ (s + |\mathbf{q}|^2) Q_0(y_{\pi i}) - |\mathbf{q}|^2 \sigma_\pi^2 [y_{\pi i}^2 Q_0(y_{\pi i}) - y_{\pi i}] \}, \quad (11)$$

where $C_{mn,i} \equiv C_{Z_{bi}\Upsilon(mS)\pi} C_{Z_{bi}\Upsilon(nS)\pi}$, $y_{\pi i} \equiv (3s_{0\pi} - s - 2m_{Z_{bi}}^2) / \kappa_\pi(s)$, and $Q_0(y)$ is a Legendre function of the second kind,

$$Q_0(y) = \frac{1}{2} \int_{-1}^1 \frac{dz}{y-z} P_0(z) = \frac{1}{2} \log \frac{y+1}{y-1} \quad (12)$$

[$P_i(z)$ refers to the standard Legendre polynomials]. Note again that we consider the Z_b -exchange diagrams only for the process involving pions. For every heavy particle, namely, the bottomonia and the Z_b states here, a non-relativistic normalization factor \sqrt{M} has been multiplied to the expressions, with M being the corresponding mass. The widths of the Z_b states are neglected in the present calculation, since their nominal values are of the order of 10 MeV and thus much smaller than the gap between their masses and the $\Upsilon(1S)\pi$ threshold.

For the D wave, in which $\pi\pi$ scattering is elastic to very good approximation in the energy range considered, we only consider the single-channel FSI, and therefore we just give the amplitudes of the process involving pions,

$$M_2^{\chi, \pi}(s) = \frac{2}{3F_\pi^2} \sqrt{m_{\Upsilon(mS)} m_{\Upsilon(nS)}} c_2 |\mathbf{q}|^2 \sigma_\pi^2, \quad (13)$$

$$\hat{M}_2^{Z_b, \pi}(s) = -\frac{5\sqrt{m_{\Upsilon(mS)} m_{\Upsilon(nS)}}}{F_\pi^2 \kappa_\pi(s)} \sum_{i=1,2} m_{Z_{bi}} C_{mn,i} [s + |\mathbf{q}|^2 - |\mathbf{q}|^2 \sigma_\pi^2 y_{\pi i}^2] [(3y_{\pi i}^2 - 1) Q_0(y_{\pi i}) - 3y_{\pi i}]. \quad (14)$$

TABLE I. All loops contributing in each diagram class. The mesons are listed as $[M1, M2, M3, M4]$; type 1(c1) and type 1(d1) refer to the corresponding diagrams in Fig. 1. Two more configurations appear as type 1(c1) in principle, namely, $[B, \bar{B}, B^*, B^*]$ and $[B^*, \bar{B}, B, B^*]$; however, their contributions to amplitude \mathcal{M}_1 , see Eq. (16), vanishes, and hence they are strongly suppressed. Flavor labels are dropped for simplicity.

Type 1(c1)	$[B, \bar{B}, B, B^*], [B, \bar{B}^*, B, B^*], [B^*, \bar{B}, B^*, B], [B, \bar{B}^*, B^*, B^*],$ $[B^*, \bar{B}, B^*, B^*], [B^*, \bar{B}^*, B, B^*], [B^*, \bar{B}^*, B^*, B], [B^*, \bar{B}^*, B^*, B^*]$
Type 1(d1)	$[B, \bar{B}, \bar{B}^*, B^*], [B, \bar{B}^*, \bar{B}, B^*], [B^*, \bar{B}^*, \bar{B}, B], [B^*, \bar{B}, \bar{B}^*, B], [B, \bar{B}^*, \bar{B}^*, B^*],$ $[B^*, \bar{B}, \bar{B}^*, B^*], [B^*, \bar{B}^*, \bar{B}, B^*], [B^*, \bar{B}^*, \bar{B}^*, B], [B^*, \bar{B}^*, \bar{B}^*, B^*].$

Now we briefly discuss the calculation of the box diagrams. There are four intermediate bottom mesons in the box diagrams Figs. 1(c1) and 1(d1), where we denote the top left one as $M1$, and the others as $M2, M3$, and $M4$, in counterclockwise order. The individual contributions are listed in Table I, with the pseudoscalar or vector content of $[M1, M2, M3, M4]$ explicitly shown. For the $\Upsilon(mS) \rightarrow \Upsilon(nS)K\bar{K}$ processes, some intermediate states can be strange bottom mesons $B_s^{(*)}$, and there are four possibilities for each $[M1, M2, M3, M4]$ given above. For simplicity, we do not list the combinations of intermediate states in the $\Upsilon(mS) \rightarrow \Upsilon(nS)K\bar{K}$ processes explicitly.

The general amplitude for the process $\Upsilon(mS)(p_a) \rightarrow \Upsilon(nS)(p_b)P(p_c)P(p_d)$ reads

$$\begin{aligned} \mathcal{M}(\Upsilon(mS) \rightarrow \Upsilon(nS)PP) \\ = \epsilon_{\Upsilon(mS)}^i \epsilon_{\Upsilon(nS)}^j \mathcal{M}^{ij}(\Upsilon(mS) \rightarrow \Upsilon(nS)PP), \end{aligned} \quad (15)$$

and $\mathcal{M}^{ij}(\Upsilon(mS) \rightarrow \Upsilon(nS)PP)$ can be decomposed as

$$\mathcal{M}^{ij}(\Upsilon(mS) \rightarrow \Upsilon(nS)PP) = \delta^{ij} \mathcal{M}_1 + \dots, \quad (16)$$

where we have omitted the remaining terms proportional to tensor structures built from the different momenta. For the loop amplitude, we have checked that the \mathcal{M}_1 term is indeed numerically dominant, which agrees with the argument that other contractions of the polarization vectors are suppressed in the heavy-quark nonrelativistic expansion. So in the following we only keep the terms proportional to $\epsilon_{\Upsilon(mS)} \cdot \epsilon_{\Upsilon(nS)}$, as we did for the tree amplitude. Details on the analytic calculation of the box diagrams are given in Appendix A.

The partial-wave projection of the loop amplitude for the $\Upsilon(mS) \rightarrow \Upsilon(nS)PP$ process can be denoted as

$$\hat{M}_l^{\text{loop}, P}(s) = g_{JHH(mS)} g_{JHH(nS)} \text{AmpBox}_l^P(s). \quad (17)$$

The analytic expressions of $\text{AmpBox}_l^P(s)$ are very involved, so in Fig. 3 we only plot the numerical results for $\Upsilon(4S) \rightarrow \Upsilon(1S, 2S)\pi^+\pi^-$ in the physical region. Note that the imaginary parts, which are due to the on-shell $B\bar{B}$ intermediate states, are tiny due to the smallness of phase space and the fact that the $B\bar{B}$ pair appears in a relative P wave.

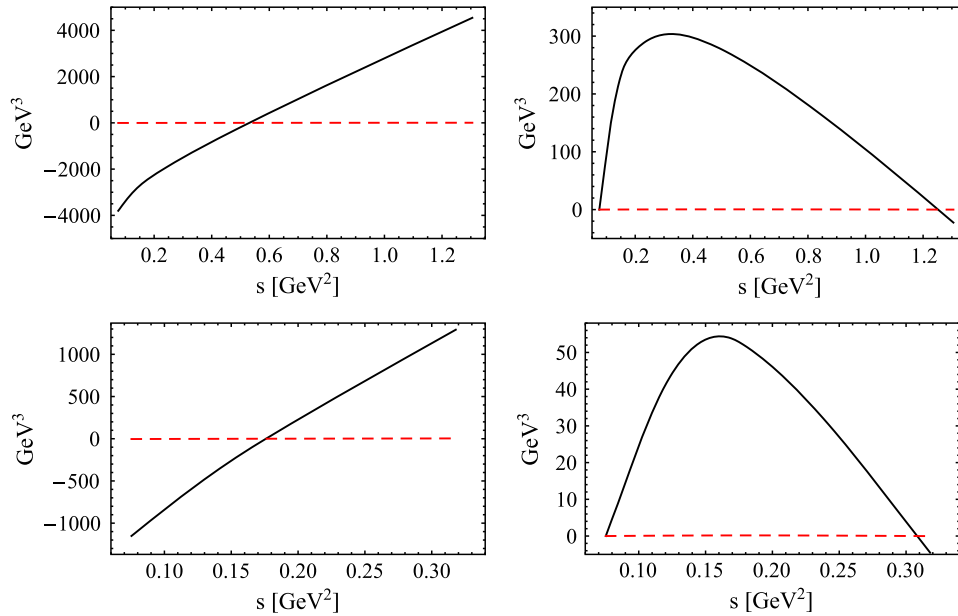


FIG. 3. The S - (left) and D -wave (right) box amplitudes in $\Upsilon(4S) \rightarrow \Upsilon(1S)\pi^+\pi^-$ (top) and $\Upsilon(4S) \rightarrow \Upsilon(2S)\pi^+\pi^-$ (bottom). The black solid and red dashed lines denote the real and imaginary parts, respectively.

D. Final-state interactions with a dispersive approach, Omnès solution

There are strong FSI in the $\pi\pi$ system especially in the isoscalar S wave, which can be taken into account model independently using dispersion theory. Based on the principles of unitarity and analyticity, dispersion theory determines the decay amplitudes up to some subtraction constants, which can be fixed by matching to the results of chiral effective theory. Since the mass difference between the $\Upsilon(4S)$ and the $\Upsilon(1S)$ is larger than the $K\bar{K}$ threshold, we consider the isospin symmetric two-channel ($\pi\pi$ and $K\bar{K}$) FSI for the dominant S -wave component, while for the D wave only the single-channel $\pi\pi$ FSI is considered.

For the $\Upsilon(mS) \rightarrow \Upsilon(nS)\pi^+\pi^-$ processes, the partial-wave expansion of the amplitude including the FSI reads

$$\mathcal{M}^{\text{full}}(s, \cos\theta) = \epsilon_{\Upsilon(nS)} \cdot \epsilon_{\Upsilon(mS)} \sum_{l=0}^{\infty} [M_l^\pi(s) + \hat{M}_l^\pi(s)] P_l(\cos\theta), \quad (18)$$

where $M_l^\pi(s)$ represents the right-hand-cut part and accounts for s -channel rescattering, and the ‘‘hat functions’’ $\hat{M}_l^\pi(s)$ contain the left-hand cuts, contributed by crossed-channel pole terms or open-flavor loop effects. In general the box diagrams contribute to both the left-hand cuts at $t, u > (m_{B^{(*)}} + m_{B^{(*)}})^2$ and right-hand cut at $s > (m_{B^{(*)}} + m_{B^{(*)}})^2$; however, this right-hand cut is far away from the physical region, so it can be safely neglected. In this study, we approximate the left-hand cuts by the sum of the Z_b -exchange diagram and the box diagrams, $\hat{M}_l^\pi(s) = \hat{M}_l^{Z_b, \pi}(s) + \hat{M}_l^{\text{loop}, \pi}(s)$. Similar methods to approximate the left-hand-cut structures by including resonance exchange (in the case of no loops) have been applied in Refs. [28–31].

Next we discuss the Omnès solution to obtain the amplitude including the FSI. For simplicity first we discuss the single-channel solution, which applies for the D -wave case. The functions $\hat{M}_l(s)$ are real along the right-hand cut, so in the elastic $\pi\pi$ rescattering region the partial-wave unitarity conditions reads

$$\text{Im}M_l(s) = [M_l(s) + \hat{M}_l(s)] \sin \delta_l^0(s) e^{-i\delta_l^0(s)}. \quad (19)$$

In the elastic region, the phases δ_l^I of the partial-wave amplitudes of isospin I and angular momentum l equal the $\pi\pi$ elastic phase shifts modulo $n\pi$, as required by Watson’s theorem [32,33]. The Omnès function is defined as [34]

$$\Omega_l^I(s) = \exp \left\{ \frac{s}{\pi} \int_{4m_\pi^2}^{\infty} \frac{dx \delta_l^I(x)}{x(x-s)} \right\}, \quad (20)$$

which obeys $\Omega_l^I(s+i\epsilon) = e^{2i\delta_l^I} \Omega_l^I(s-i\epsilon)$. Using the Omnès function, the solution of Eq. (19) can be obtained [8,35],

$$M_l(s) = \Omega_l^0(s) \left\{ P_l^{n-1}(s) + \frac{s^n}{\pi} \int_{4m_\pi^2}^{\infty} \frac{dx \hat{M}_l(x) \sin \delta_l^0(x)}{x^n |\Omega_l^0(x)|(x-s)} \right\}, \quad (21)$$

where the polynomial $P_l^{n-1}(s)$ is a subtraction function. For the D -wave phase shift $\delta_2^0(s)$, we use the result given by the Madrid-Kraków collaboration [36], and smoothly continue it to π for $s \rightarrow \infty$.

For the S wave, we take into account the two-channel rescattering effects. Along the right-hand cut, the two-channel unitarity conditions reads

$$\text{Im}\mathbf{M}_0(s) = 2iT_0^{0*}(s)\Sigma(s)[\mathbf{M}_0(s) + \hat{\mathbf{M}}_0(s)], \quad (22)$$

where the two-dimensional vectors $\mathbf{M}_0(s)$ and $\hat{\mathbf{M}}_0(s)$ contain the right-hand and the left-hand-cut parts of both the $\pi\pi$ and the $K\bar{K}$ final states, respectively,

$$\mathbf{M}_0(s) = \begin{pmatrix} M_0^\pi(s) \\ \frac{2}{\sqrt{3}} M_0^K(s) \end{pmatrix}, \quad \hat{\mathbf{M}}_0(s) = \begin{pmatrix} \hat{M}_0^\pi(s) \\ \frac{2}{\sqrt{3}} \hat{M}_0^K(s) \end{pmatrix}. \quad (23)$$

The two-dimensional matrices $T_0^0(s)$ and $\Sigma(s)$ are

$$T_0^0(s) = \begin{pmatrix} \frac{\eta_0^0(s)e^{2i\delta_0^0(s)}-1}{2i\sigma_\pi(s)} & |g_0^0(s)|e^{i\psi_0^0(s)} \\ |g_0^0(s)|e^{i\psi_0^0(s)} & \frac{\eta_0^0(s)e^{2i(\psi_0^0(s)-\delta_0^0(s))}-1}{2i\sigma_K(s)} \end{pmatrix} \quad (24)$$

and $\Sigma(s) \equiv \text{diag}(\sigma_\pi(s)\theta(s-4m_\pi^2), \sigma_K(s)\theta(s-4m_K^2))$. There are three input functions in the $T_0^0(s)$ matrix: the $\pi\pi S$ -wave isoscalar phase shift $\delta_0^0(s)$, for which we use the result from the Roy equation analysis in Ref. [37]; and the $\pi\pi \rightarrow K\bar{K}$ S -wave amplitude $g_0^0(s) = |g_0^0(s)|e^{i\psi_0^0(s)}$ with modulus and phase, for which the results based on the Roy-Steiner approach in Ref. [38] are used. These inputs are used below the appearance of additional inelasticities from 4π intermediate states, namely, up to $\sqrt{s_0} = 1.3$ GeV [the $f_0(1370)$ resonance is known to have a significant coupling to 4π [39]]. Above s_0 , the phases $\delta_0^0(s)$ and ψ_0^0 are guided smoothly to 2π [40],

$$\delta(s) = 2\pi + (\delta(s_0) - 2\pi) \frac{2}{1 + (\frac{s}{s_0})^{3/2}}. \quad (25)$$

The inelasticity $\eta_0^0(s)$ in Eq. (24) is related to the modulus $|g_0^0(s)|$ by

$$\eta_0^0(s) = \sqrt{1 - 4\sigma_\pi(s)\sigma_K(s)|g_0^0(s)|^2\theta(s-4m_K^2)}. \quad (26)$$

The numerical solution of the homogeneous two-channel unitarity relation

$$\text{Im}\Omega(s) = 2iT_0^{0*}(s)\Sigma(s)\Omega(s), \quad \Omega(0) = 1, \quad (27)$$

has been computed in Refs. [40–43]. Using $\Omega(s)$, the solution of the inhomogeneous two-channel unitarity condition in Eq. (22) is given by

$$\mathbf{M}_0(s) = \Omega(s) \left\{ \mathbf{P}^{n-1}(s) + \frac{s^n}{\pi} \int_{4m_\pi^2}^{\infty} \frac{dx}{x^n} \times \frac{\Omega^{-1}(x)T(x)\Sigma(x)\hat{\mathbf{M}}_0(x)}{x-s} \right\}. \quad (28)$$

To determine the required number of subtractions that guarantees that the dispersive integrals in Eqs. (21) and (28) converge, we need to investigate the high-energy behavior of the integrand. First it is known that for the single-channel Omnès function defined in Eq. (20), it falls off asymptotically as s^{-k} if the phase shift $\delta_l^f(s)$ approaches $k\pi$ at high energies. Since the D -wave $\pi\pi$ phase shift, $\delta_2^0(s)$, reaches π for high energies, we have $\Omega_2^0(s) \sim 1/s$ for large s . Second, the high-energy behavior of the two-channel Omnès function has been analyzed in Ref. [40], and the $1/s$ asymptotic behavior of $\Omega_l^f(s)$ is ensured by the asymptotic condition $\sum \delta_l^f(s) \geq 2\pi$ for $s \rightarrow \infty$, where $\sum \delta_l^f(s)$ is the sum of the eigen phase shifts. Third, we have checked that in an intermediate energy range of $1 \text{ GeV}^2 \lesssim s \ll m_\Upsilon^2$, both the inhomogeneities contributed by the Z_b -exchange term and the box graph term grow at most linearly in s . So we conclude that in the dispersive representations for $M_2(s)$ and $\mathbf{M}_0(s)$, three subtractions are sufficient to make the dispersive integrals convergent.

At low energies, the amplitudes $M_2(s)$ and $\mathbf{M}_0(s)$ should match to the results of chiral perturbation theory. Namely, in the limit of switching off the final-state interactions, $\Omega_2^0(s) = 1$ and $\Omega(0) = 1$, the subtraction functions agree with the chiral representations given in Eqs. (10) and (13). Since both $M_0^K(s)$ and $M_2^K(s)$ grow no faster than $\sim s^2$, they can be covered by the degree of the subtractions. Therefore, for the D wave, the integral equation takes the form

$$M_2^\pi(s) = \Omega_2^0(s) \left\{ M_2^{\pi,\pi}(s) + \frac{s^3}{\pi} \int_{4m_\pi^2}^{\infty} \frac{dx}{x^3} \frac{\hat{M}_2^\pi(x) \sin \delta_2^0(x)}{|\Omega_2^0(x)|(x-s)} \right\}. \quad (29)$$

For the S wave, the integral equation reads

$$\mathbf{M}_0(s) = \Omega(s) \left\{ \mathbf{M}_0^K(s) + \frac{s^3}{\pi} \int_{4m_\pi^2}^{\infty} \frac{dx}{x^3} \times \frac{\Omega^{-1}(x)T(x)\Sigma(x)\hat{\mathbf{M}}_0(x)}{x-s} \right\}, \quad (30)$$

where $\mathbf{M}_0^K(s) = (M_0^{\pi,K}(s), 2/\sqrt{3}M_0^{\pi,K}(s))^T$.

The differential decay width for $\Upsilon(mS) \rightarrow \Upsilon(nS)\pi^+\pi^-$ with respect to the $\pi\pi$ invariant mass and the helicity angle reads

$$\frac{d\Gamma}{d\sqrt{s}d\cos\theta} = \frac{\sqrt{s}\sigma_\pi|\mathbf{q}|}{128\pi^3 m_{\Upsilon(mS)}^2} |M_0^\pi + \hat{M}_0^\pi + (M_2^\pi + \hat{M}_2^\pi)P_2(\cos\theta)|^2. \quad (31)$$

III. PHENOMENOLOGICAL DISCUSSION

The experimental data considered in this work are the $\pi\pi$ invariant mass distributions of the $\Upsilon(4S) \rightarrow \Upsilon(1S, 2S)\pi^+\pi^-$ decays measured by the *BABAR* [44] and Belle collaborations [45].

The chiral coupling constants c_i in Eq. (1) are different for the two decays $\Upsilon(4S) \rightarrow \Upsilon(1S)\pi^+\pi^-$ and $\Upsilon(4S) \rightarrow \Upsilon(2S)\pi^+\pi^-$, since there is no symmetry connecting the bottomonium states with different radial excitations. The mass difference between the two Z_b states is much smaller than the difference between their masses and the $\Upsilon(lS)\pi(l=1, 2)$ thresholds as well as $m_{\Upsilon(4S)} - m_\pi$; they have the same quantum numbers and thus the same coupling structure as given by Eq. (3). So the $Z_b(10610)$ and $Z_b(10650)$ contributions are strongly correlated in the fit, and it is very difficult to distinguish their effects from each other in the processes studied in this work. Therefore we only use one Z_b , the $Z_b(10610)$, in our fit by setting $C_{nm,2} = 0$ as in our previous analysis of $\Upsilon(3S) \rightarrow \Upsilon(1, 2S)\pi\pi$ [8]. For the input mass of the $Z_b(10610)$, we use the heavy-quark spin symmetry conserving result given in Ref. [46]. The value of $g_{JHH(4S)}$ is extracted from the measured open-bottom decay widths of the $\Upsilon(4S)$, $g_{JHH(4S)} = 1.43 \text{ GeV}^{-3/2}$.

For each $\Upsilon(4S) \rightarrow \Upsilon(nS)\pi\pi(n=1, 2)$ process, the unknown parameters are c_1 and c_2 corresponding to the chiral contact $\Upsilon\Upsilon'\Phi\Phi$ coupling, $C_{4n,1}$ related to the Z_b -exchange mechanism, and $g_{JHH(nS)}$ for the box diagrams. To illustrate the effects of the Z_b -exchange and box graph mechanisms, we perform several fits by choosing different strategies. Fit I only includes the chiral contact c_i terms; fit II adds the Z_b -exchange terms to them. Fit III includes the chiral contact c_i terms and the box diagrams, and finally fit IV takes all of the contact c_i terms, the Z_b exchange, and the box diagrams into account. The FSI is included in all fits. In Fig. 4, the fitted results of fits I–IV are shown as the green dash-dot-dotted, red dashed, blue dot-dashed, and black solid lines, respectively. The fitted parameters as well as the $\chi^2/\text{d.o.f.}$ of our best fit, fit IV, are shown in Table II. We find very different values for the parameters c_1 and c_2 from fitting the data of transitions between different $\Upsilon(lS)$ states. These low-energy constants parametrize the non-perturbative QCD matrix elements of gluonic operators between the initial and final bottomonia. For different initial and final Υ states, these parameters are not related to

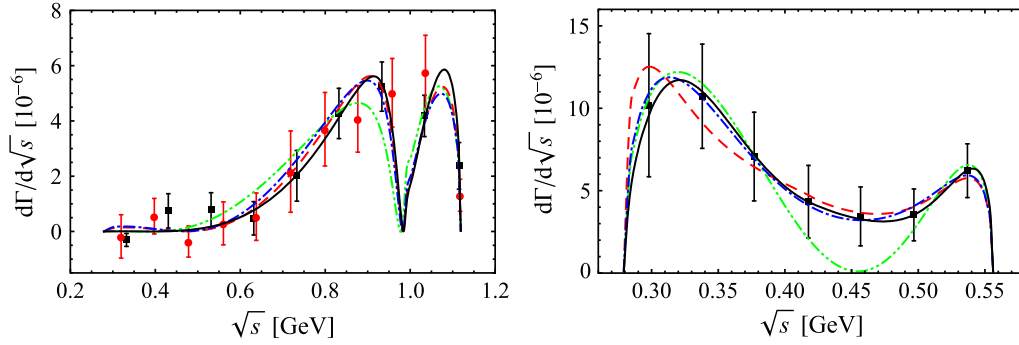


FIG. 4. Fit results of the $\pi\pi$ invariant mass spectra for the decays $\Upsilon(4S) \rightarrow \Upsilon(1S)\pi^+\pi^-$ (left) and $\Upsilon(4S) \rightarrow \Upsilon(2S)\pi^+\pi^-$ (right). The solid squares and solid circles denote the data from the *BABAR* Collaboration [44] and Belle Collaboration [45], respectively. Fit I (green dash-dot-dotted) only includes the chiral contact terms c_i ; fit II (red dashed) includes chiral contact terms and the Z_b -exchange term; fit III (blue dot-dashed) includes chiral contact terms and box diagrams; fit IV (black solid) includes the contact terms c_i , the Z_b -exchange term, and the box diagrams. The FSI is included in all fits.

each other at the hadronic level, and can well be very different. In principle, the parameter values from the fit in this paper cannot be directly compared with those in Ref. [8], which do not include the box diagrams when analyzing the $\Upsilon(3S)$ and $\Upsilon(2S)$ dipion transitions. We thus made a new fit to the decay $\Upsilon(3S) \rightarrow \Upsilon(1S)\pi\pi$ studied therein. It turns out that the values of c_1 and c_2 decrease only by around 35% in comparison with those given in Table I of Ref. [8]. Our fittings turn out to indicate the following hierarchy: $|c_{1,2}^{4 \rightarrow 1}| \ll |c_{1,2}^{4 \rightarrow 2}| \lesssim |c_{1,2}^{3 \rightarrow 1}| \ll |c_{1,2}^{3 \rightarrow 2}|$. This may be understood from the node structure of the Υ wave functions: for the processes with the same initial Υ state, the larger the difference between the principal quantum numbers, the smaller the gluonic matrix elements and thus the magnitude of the parameters. Note that the total χ^2 value for the transition $\Upsilon(4S) \rightarrow \Upsilon(2S)\pi^+\pi^-$ is very low, $\chi^2/\text{d.o.f} = 0.01$. This small number reflects the observation that the fluctuation in the data appears to be significantly smaller than what the error bars allow for, which indicates that they might well be dominated by systematics.

Using the central values of the parameters in the best fit, in Fig. 5 we plot the moduli of the S - and D -wave amplitudes from the c_i terms, the $Z_b(10610)$ state, and the box graphs for the processes $\Upsilon(4S) \rightarrow \Upsilon(1S)\pi^+\pi^-$ and

TABLE II. Fit parameters from the best fits of the $\Upsilon(4S) \rightarrow \Upsilon(nS)\pi\pi$ ($n = 1, 2$) processes.

	$\Upsilon(4S) \rightarrow \Upsilon(1S)\pi^+\pi^-$	$\Upsilon(4S) \rightarrow \Upsilon(2S)\pi^+\pi^-$
$c_1(\text{GeV}^{-1})$	$(9.8 \pm 1.0) \times 10^{-4}$	$(1.2 \pm 0.6) \times 10^{-1}$
$c_2(\text{GeV}^{-1})$	$(-1.6 \pm 1.1) \times 10^{-4}$	$(-1.0 \pm 0.6) \times 10^{-1}$
$C_{4n,1}$	$(2.6 \pm 1.3) \times 10^{-4}$	$(-3.2 \pm 1.8) \times 10^{-2}$
$g_{J_{HH}(nS)}(\text{GeV}^{-\frac{3}{2}})$	$(8.6 \pm 6.1) \times 10^{-5}$	$(1.7 \pm 0.8) \times 10^{-2}$
$\chi^2/\text{d.o.f}$	$10.45/(20 - 4) = 0.65$	$0.04/(7 - 4) = 0.01$

$\Upsilon(4S) \rightarrow \Upsilon(2S)\pi^+\pi^-$, respectively. In addition, in Fig. 6 we show the resulting theoretical predictions for the angular distributions.

As shown in Fig. 4, including the Z_b -exchange and the box graph contributions improves the fit quality for $\Upsilon(4S) \rightarrow \Upsilon(1S)\pi^+\pi^-$ only marginally, mainly in the region around 1 GeV. However, for $\Upsilon(4S) \rightarrow \Upsilon(2S)\pi^+\pi^-$, the fit quality increases significantly when considering either of those two mechanisms (or both). Loop effects were already studied in the 3P_0 quark-pair-creation model in Ref. [47], and found to be tiny for $\Upsilon(3S, 2S) \rightarrow \Upsilon(2S, 1S)\pi^+\pi^-$. This is probably due to the fact that $\Upsilon(3S, 2S)$ are too far below the $B\bar{B}$ threshold. This situation is expected to change for the $\Upsilon(4S)$, with the open-bottom channels contributing significantly to its decay rate. In Fig. 5, one observes that for the dominant S -wave amplitudes, the contributions from the c_i terms, from the Z_b -exchange term, and from the box diagram term are all of the same order. Especially, for the decay $\Upsilon(4S) \rightarrow \Upsilon(1S)\pi^+\pi^-$, the box graphs and the Z_b exchange play a major role in the energy range around 0.95 GeV, and account for the better description of the data there. Note that the contribution of loops including B_s mesons, producing kaons that subsequently rescatter into a pion pair, is entirely negligible: in the NREFT formalism, these graphs vanish at the $K\bar{K}$ threshold. For the D wave, the contributions from Z_b exchange and the box graphs are much smaller than that from the c_i terms. We should mention that the plots in Fig. 5 correspond to using the central values of the best fit parameters. The shapes of the curves corresponding to the box diagrams and the Z_b -exchange terms are similar; however, their relative strength is not very meaningful because there is a strong correlation in the fit between the parameters $C_{41,1}$ and $J_{J_{HH}(1S)}$. This can be easily seen from the fact that the curves for fits II and III are very similar to each other in Fig. 4 (left), which means that the Z_b -exchange and box terms can hardly be distinguished in the $\pi\pi$ invariant mass distribution of the transition $\Upsilon(4S) \rightarrow \Upsilon(1S)\pi^+\pi^-$.

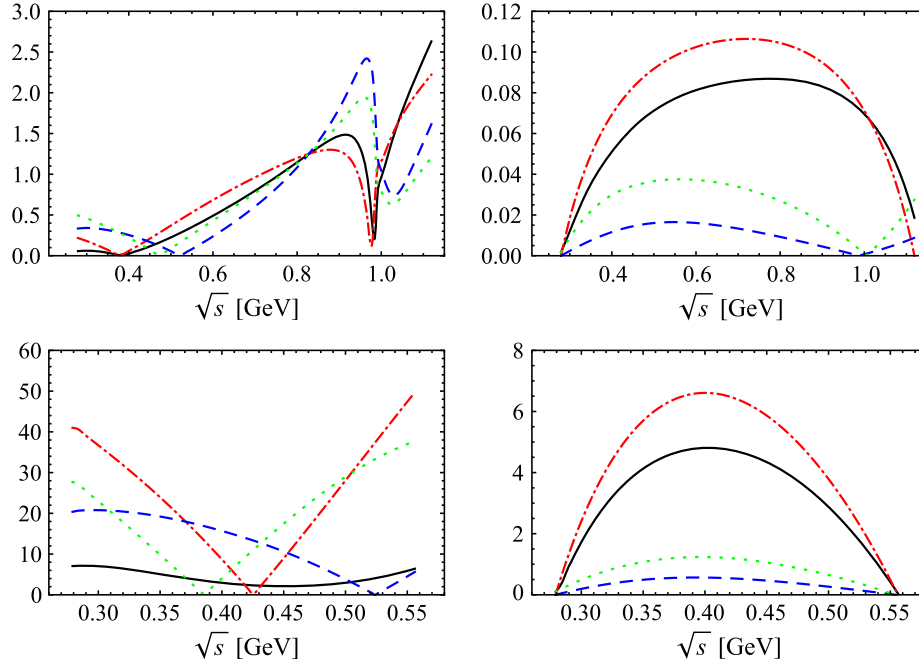


FIG. 5. Moduli of the S - (left) and D -wave (right) amplitudes in $\Upsilon(4S) \rightarrow \Upsilon(1S)\pi^+\pi^-$ (top) and $\Upsilon(4S) \rightarrow \Upsilon(2S)\pi^+\pi^-$ (bottom). The black solid lines represent our best fit results, while the red dot-dashed, blue dashed, and green dotted lines correspond to the contributions from the c_i terms, the $Z_b(10610)$, and the box diagrams, respectively.

Notice that in Refs. [48,49], the loop contribution of the sequential process $\Upsilon(4S) \rightarrow B\bar{B} \rightarrow \Upsilon(nS)S \rightarrow \Upsilon(nS)\pi^+\pi^- \times (n=1,2)$, where the scalar S can correspond to the $f_0(500)$ and the $f_0(980)$, has been considered. This kind of loop topology can be described by Fig. 2(a) including FSIs, which is suppressed compared to the box graphs in NREFT. In our scheme, the FSIs are taken into account in a model-independent way, and we do not have to specify the contributing scalar resonances. Another merit of our calculation is that, instead of only obtaining the absorptive part of the loops by using Cutkosky rules [48,49], we completely compute both their real and imaginary parts.

An interesting feature of the $\pi\pi$ invariant mass distribution of $\Upsilon(4S) \rightarrow \Upsilon(1S)\pi^+\pi^-$ is that the older Belle data from Ref. [50] hint at a two-peak structure in the range of $m_{\pi^+\pi^-} = 0.8 \dots 1.2$ GeV, while the later measurements given in Refs. [44,45] do not display such a feature in

any obvious way. As the mass difference between $\Upsilon(4S)$ and $\Upsilon(1S)$ is about 1.12 GeV, the isoscalar-scalar $f_0(980)$ meson, which couples strongly to $\pi\pi$, should be visible in the spectrum. With the FSI described reliably in the dispersive approach, we see that the $f_0(980)$ indeed accounts for a dip at its mass, and a two-peak structure is naturally produced. A possible reason why such a two-peak structure is not observed in Refs. [44,45] may be the wide energy bins used in these experimental measurements. The fact that the $f_0(980)$ should be manifest in the $\pi\pi$ invariant mass distribution of $\Upsilon(4S) \rightarrow \Upsilon(1S)\pi^+\pi^-$ has already been emphasized in Ref. [7]. The dip caused by the $f_0(980)$ is also present in the calculation of Ref. [51].

For the $\Upsilon(4S) \rightarrow \Upsilon(2S)\pi^+\pi^-$ process, it is known that the two-hump behavior in the $\pi\pi$ invariant mass spectra is incompatible with the prediction from the QCD multipole expansion, resembling the case of $\Upsilon(3S) \rightarrow \Upsilon(1S)\pi\pi$

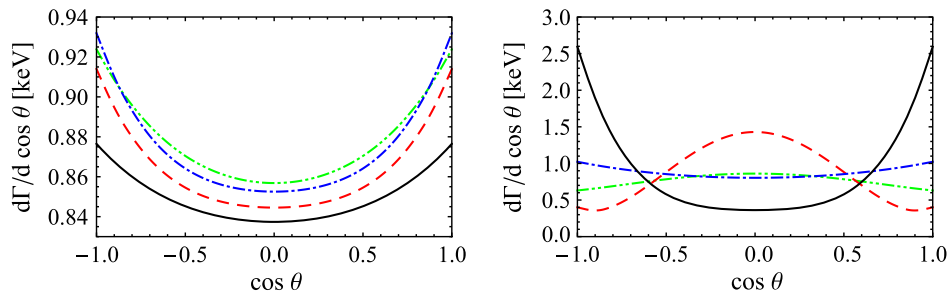


FIG. 6. Theoretical predictions of the helicity angular distributions for the decays $\Upsilon(4S) \rightarrow \Upsilon(1S)\pi^+\pi^-$ (left) and $\Upsilon(4S) \rightarrow \Upsilon(2S)\pi^+\pi^-$ (right). The line style is as in Fig. 4.

[5,8,47]. In the formalism outlined above, the original formulation of the QCD multipole expansion appears by including only the tree-level c_i terms, however, omitting the $\pi\pi$ FSIs. As shown by the blue dot-dashed line in the right panel of Fig. 4, including the final-state interaction can roughly reproduce a two-hump structure. However, it produces a 0 in the amplitude inside the physical region and the agreement with the data is not very convincing. This feature was also observed in our previous study of $\Upsilon(3S) \rightarrow \Upsilon(1S)\pi\pi$, where, however, a simultaneous fit of the $\pi\pi$ invariant mass and the helicity angular distributions cannot reproduce the two-hump behavior in the dipion mass spectra by only using the c_i terms [8]. The angular distribution data are therefore important to distinguish the effects of different mechanisms. In Fig. 6, the theoretical predictions of the helicity angular distributions in different fit scenarios are shown. For $\Upsilon(4S) \rightarrow \Upsilon(2S)\pi^+\pi^-$, the angular distributions are distinctly different when including the Z_b -exchange and box graph terms; hence these results can be used to check their effects when experimental data become available in the future.

Using the fit parameters given in Table II, we can predict the decay width of $\Upsilon(4S) \rightarrow \Upsilon(1S)K^+K^-$, as well as the corresponding $K\bar{K}$ invariant mass distribution. The relevant Feynman diagrams can be obtained by replacing all external pions by kaons in Fig. 1, but without diagram (b1) due to the absence of a $Z_b\Upsilon K$ vertex. The Z_b contributes also to $K\bar{K}$ through diagram (b2) due to the final-state interactions that, especially around the $K\bar{K}$ threshold, provide strong

$\pi\pi \rightarrow K\bar{K}$ transitions. Most ingredients of the amplitude of the $\Upsilon(4S) \rightarrow \Upsilon(1S)K^+K^-$ process have been given in Sec. II. We omit the $K\bar{K} D$ wave, which is negligible due to its strong near-threshold suppression. Within 1σ uncertainties, the prediction of the decay width of $\Upsilon(4S) \rightarrow \Upsilon(1S)K^+K^-$ is

$$\Gamma_{\Upsilon(4S) \rightarrow \Upsilon(1S)K^+K^-} = 0.18_{-0.09}^{+0.21} \text{ keV}, \quad (32)$$

corresponding to a branching fraction of $0.9_{-0.4}^{+1.0} \times 10^{-5}$, and the dikaon invariant mass spectrum is given in Fig. 7 (top left). The rapid rise of the $K\bar{K}$ invariant mass distribution in the near-threshold region is a result of the $f_0(980)$, in line with the dip around 1 GeV in Fig. 4. Like the $\Upsilon(4S) \rightarrow \Upsilon(1S)\pi^+\pi^-$ process, there is a strong correlation between the Z_b -exchange terms and the box diagrams in the $\Upsilon(4S) \rightarrow \Upsilon(1S)K^+K^-$ process, and in Fig. 7 we also plot the contributions from the c_i terms (top right), the $Z_b(10610)$ state plus box graphs (bottom left), and their interference (bottom right), respectively. One finds that for the central values of the theoretical predictions, the Z_b -exchange term and the box graphs nearly cancel each other, and the total line shape is quite similar to the c_i terms only. Both the rapid rise in the $m_{K\bar{K}}$ distribution and the nontrivial structure in the large $m_{\pi\pi}$ region of the dipion invariant mass distribution are due to the final-state interactions between the light mesons, depicted in Figs. 1(c1), 1(d1), and 1(a2)–1(d2), which receive contributions from both the Z_b -exchange and box diagrams. As a result, their strong correlation in the fit to the data of the dipion transitions

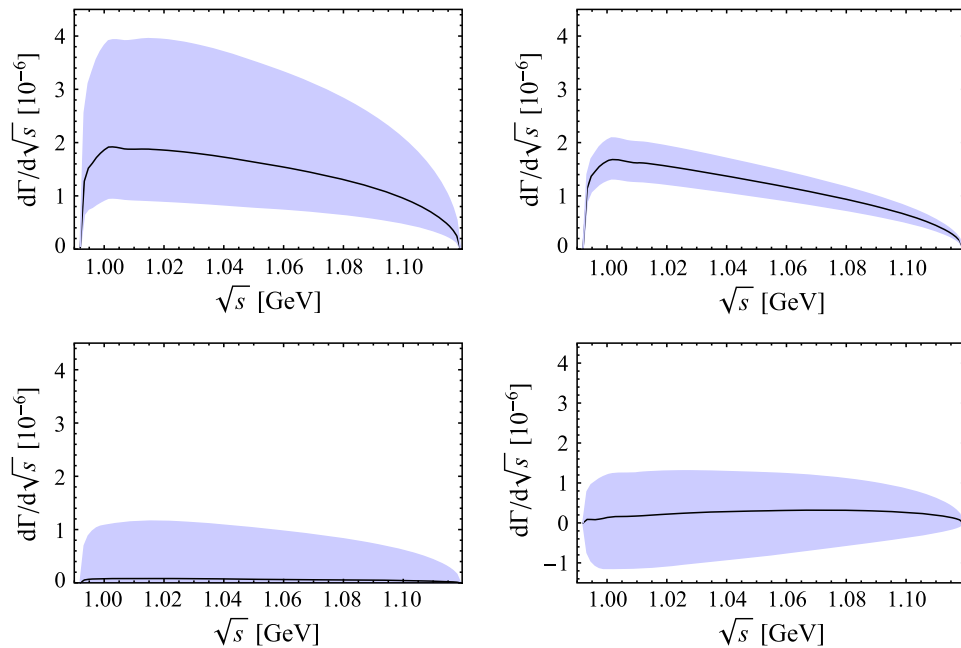


FIG. 7. Theoretical prediction of the $K\bar{K}$ invariant mass spectrum for the decay $\Upsilon(4S) \rightarrow \Upsilon(1S)K^+K^-$ (top left). The contributions from the c_i terms (top right), the $Z_b(10610)$ state plus box graphs (bottom left), and their interference (bottom right) are also depicted. The shaded areas correspond to the error band.

leads to the significant cancellation in the prediction of the $m_{K\bar{K}}$ distribution. The large spread mainly comes from the uncertainties of $Z_b(10610)$ plus box graphs, and the interference term. These predictions encourage future experimental measurements in this channel.

IV. CONCLUSIONS

We have studied the effects of Z_b exchange and bottom meson loops in the decays $\Upsilon(4S) \rightarrow \Upsilon(nS)\pi\pi$ ($n = 1, 2$). The bottom meson loops are treated in the NREFT scheme, in which the power counting rules indicate that the box diagrams are dominant. The strong FSIs, especially the coupled-channel FSI in the S wave, are taken into account model independently by using dispersion theory. The forms of the subtraction functions are obtained by matching to the leading chiral contact terms. Through fitting the data of the $\pi\pi$ invariant mass spectra, the couplings of the $\Upsilon\Upsilon'\pi\pi$ and $\Upsilon B^{(*)}B^{(*)}$ vertices, as well as the product of couplings of the $Z_b\Upsilon\pi$ and $Z_b\Upsilon'\pi$ vertices are determined (where Υ and Υ' denote the final- and initial-state bottomonia). For the dominant S -wave component, it is found that the contributions from Z_b exchange, the loops, and the chiral contact term are of the same order. For $\Upsilon(4S) \rightarrow \Upsilon(2S)\pi^+\pi^-$, including the Z_b -exchange term and the bottom meson loops naturally describes the two-hump behavior in the $\pi\pi$ invariant mass distribution. Unfortunately, the present data are insufficient to distinguish between the effects of the Z_b exchange and the bottom meson loops. We provide theoretical predictions of the helicity angular distributions, which may be useful to identify the effects of Z_b exchange and bottom meson loops with future experimental data. For the $\Upsilon(4S) \rightarrow \Upsilon(1S)\pi^+\pi^-$ decay, we expect that there is a dip in the $\pi\pi$ spectrum around 1 GeV, caused by the opening of the $K\bar{K}$ channel near the $f_0(980)$ resonance. This dip has probably not been observed yet in the present experimental data yet due to lack of sufficiently precise energy resolution. Improved data to resolve this issue are eagerly awaited. We also predict the decay width and the $K\bar{K}$ invariant mass distribution of the $\Upsilon(4S) \rightarrow \Upsilon(1S)K^+K^-$ process, demonstrating the usefulness of this additional measurement that should be feasible at Belle II.

ACKNOWLEDGMENTS

We are grateful to Zhi-Hui Guo, Claudia Patrignani, and Qian Wang for helpful discussions, and to Roman Mizuk for the proposal to add the investigation of the K^+K^- final state. This work is supported in part by Natural Science Foundation of China (NSFC) and Deutsche Forschungsgemeinschaft (DFG) through funds provided to the Sino-German Collaborative Research Center (CRC) 110 ‘‘Symmetries and the Emergence of Structure in QCD’’ (NSFC Grant No. 11621131001 and DFG Grant No. TRR110), by NSFC (Grant No. 11647601), by the Thousand Talents Plan for Young Professionals, by the CAS Key Research Program of Frontier Sciences (Grant No. QYZDB-SSW-SYS013), and by the CAS President’s International Fellowship Initiative (PIFI, Grant No. 2015VMA076). M. C. also acknowledges support by the Spanish Ministerio de Economía y Competitividad (MINECO) under Grant No. MDM-2014-0369 of ICCUB (Unidad de Excelencia María de Maeztu), and, with additional European Fondo Europeo de Desarrollo Regional (FEDER) funds, under Contract No. FIS2014-54762-P as well as support from the Generalitat de Catalunya Contract No. 2014SGR-401, and from the Spanish Excellence Network on Hadronic Physics Grant No. FIS2014-57026-REDT.

APPENDIX: REMARKS ON THE BOX DIAGRAMS AND FOUR-POINT INTEGRALS

In this appendix, we discuss the calculation of the amplitudes that involve four-point loop integrals in some detail. We start by discussing the parametrization and simplification of scalar four-point integrals. Then we introduce a tensor reduction scheme to deal with higher-rank integrals. Finally, we give the leading part of the corresponding integrals (proportional to $\epsilon_{\Upsilon'} \cdot \epsilon_{\Upsilon}$) for the possible intermediate bottom mesons.

1. Scalar four-point integrals

Because of the simpler structure we begin with the first topology as shown in Fig. 8. The corresponding scalar integral, evaluated for the initial bottomonium at rest [$p = (M, \mathbf{0})$] and labeled $J^{(0c)}$ to be consistent with Fig. 1, reads

$$\begin{aligned}
 J^{(0c)} &\equiv i \int \frac{d^4l}{(2\pi)^4} \frac{1}{[l^2 - m_1^2 + i\epsilon][(p-l)^2 - m_2^2 + i\epsilon][(l-q_1-q_2)^2 - m_3^2 + i\epsilon][(l-q_1)^2 - m_4^2 + i\epsilon]} \\
 &\simeq \frac{-i}{16m_1m_2m_3m_4} \int \frac{d^4l}{(2\pi)^4} \frac{1}{[l^0 - \frac{l^2}{2m_1} - m_1 + i\epsilon][l^0 - M + \frac{l^2}{2m_2} + m_2 - i\epsilon]} \\
 &\quad \times \frac{1}{[l^0 - q_1^0 - q_2^0 - \frac{(1+\mathbf{q})^2}{2m_3} - m_3 + i\epsilon][l^0 - q_1^0 - \frac{(1-\mathbf{q}_1)^2}{2m_4} - m_4 + i\epsilon]}.
 \end{aligned} \tag{A1}$$

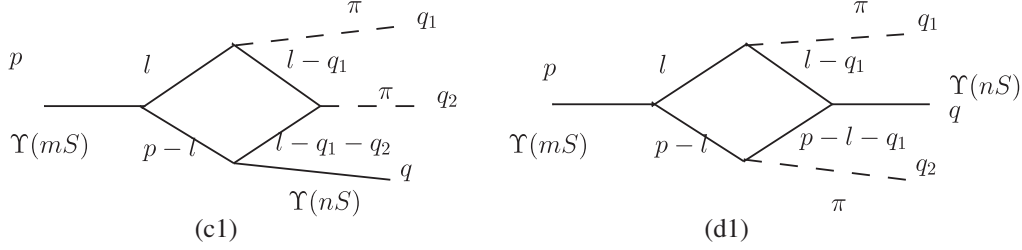


FIG. 8. Kinematics used in the calculation of the four-point integrals.

Performing the contour integration is straightforward since only one pole is located in the upper half-plane. We find

$$-\frac{\mu_{12}\mu_{23}\mu_{24}}{2m_1m_2m_3m_4} \int \frac{d^3l}{(2\pi)^3} \frac{1}{[\mathbf{l}^2 + c_{12} - i\epsilon][\mathbf{l}^2 + 2\frac{\mu_{23}}{m_3}\mathbf{l} \cdot \mathbf{q} + c_{23} - i\epsilon][\mathbf{l}^2 - 2\frac{\mu_{24}}{m_4}\mathbf{l} \cdot \mathbf{q}_1 + c_{24} - i\epsilon]}, \quad (\text{A2})$$

where we defined

$$c_{12} \equiv 2\mu_{12}(m_1 + m_2 - M), \quad c_{23} \equiv 2\mu_{23} \left(m_2 + m_3 - M + q_1^0 + q_2^0 + \frac{\mathbf{q}^2}{2m_3} \right),$$

$$c_{24} \equiv 2\mu_{24} \left(m_2 + m_4 - M + q_1^0 + \frac{\mathbf{q}_1^2}{2m_4} \right), \quad \mu_{ij} = \frac{m_i m_j}{m_i + m_j}. \quad (\text{A3})$$

For the second topology we immediately find

$$J^{(0d)} \equiv i \int \frac{d^4l}{(2\pi)^4} \frac{1}{[l^2 - m_1^2 + i\epsilon][(p-l)^2 - m_2^2 + i\epsilon][(p-q_2-l)^2 - m_3^2 + i\epsilon][(l-q_1)^2 - m_4^2 + i\epsilon]}$$

$$\simeq \frac{-i}{16m_1m_2m_3m_4} \int \frac{d^4l}{(2\pi)^4} \frac{1}{[l^0 - \frac{l^2}{2m_1} - m_1 + i\epsilon][l^0 - M + \frac{l^2}{2m_2} + m_2 - i\epsilon]}$$

$$\times \frac{1}{[l^0 + q_2^0 - M + \frac{(l+\mathbf{q}_2)^2}{2m_3} + m_3 - i\epsilon][l^0 - q_1^0 - \frac{(l-\mathbf{q}_1)^2}{2m_4} - m_4 + i\epsilon]}. \quad (\text{A4})$$

Here the possibility for two different cuts to go on shell leads to a slightly more complicated three-dimensional integral

$$-\frac{\mu_{12}\mu_{34}}{2m_1m_2m_3m_4} \int \frac{d^3l}{(2\pi)^3} \frac{1}{[\mathbf{l}^2 + d_{12} - i\epsilon][\mathbf{l}^2 - 2\frac{\mu_{34}}{m_4}\mathbf{l} \cdot \mathbf{q}_1 - 2\frac{\mu_{34}}{m_3}\mathbf{l} \cdot \mathbf{q}_2 + d_{34} - i\epsilon]}$$

$$\times \left[\frac{\mu_{24}}{[\mathbf{l}^2 - 2\frac{\mu_{24}}{m_4}\mathbf{l} \cdot \mathbf{q}_1 + d_{24} - i\epsilon]} + \frac{\mu_{13}}{[\mathbf{l}^2 + 2\frac{\mu_{13}}{m_3}\mathbf{l} \cdot \mathbf{q}_2 + d_{13} - i\epsilon]} \right], \quad (\text{A5})$$

where we defined

$$d_{12} \equiv 2\mu_{12}(m_1 + m_2 - M), \quad d_{34} \equiv 2\mu_{34} \left(m_3 + m_4 - q^0 + \frac{\mathbf{q}_1^2}{2m_4} + \frac{\mathbf{q}_2^2}{2m_3} \right),$$

$$d_{24} \equiv 2\mu_{24} \left(m_2 + m_4 - M + q_1^0 + \frac{\mathbf{q}_1^2}{2m_4} \right), \quad d_{13} \equiv 2\mu_{13} \left(m_1 + m_3 - M + q_2^0 + \frac{\mathbf{q}_2^2}{2m_3} \right). \quad (\text{A6})$$

In both cases the remaining three-dimensional momentum integration needs to be carried out numerically.

2. Tensor reduction

Since each of the interactions of an Υ with a pair of bottom mesons scales with the momentum of the latter we have to deal with

$$\frac{-\mu_{12}\mu_{23}\mu_{24}}{2m_1m_2m_3m_4} \int \frac{d^3l}{(2\pi)^3} \frac{f(l)}{[\mathbf{l}^2 + c_{12} - i\epsilon][\mathbf{l}^2 + 2\frac{\mu_{23}}{m_3}\mathbf{l} \cdot \mathbf{q} + c_{23} - i\epsilon][\mathbf{l}^2 - 2\frac{\mu_{24}}{m_4}\mathbf{l} \cdot \mathbf{q}_1 + c_{24} - i\epsilon]}, \quad (\text{A7})$$

where $f(l) = \{1, l^i, l^i l^j\}$ for the fundamental scalar, vector, and tensor integrals, respectively. Using the momentum of the final state Υ , \mathbf{q} , and $\mathbf{q}_\perp = \mathbf{q}_1 - \mathbf{q}(\mathbf{q} \cdot \mathbf{q}_1)/\mathbf{q}^2$, a convenient parametrization reads

$$J^{(1)i} = \frac{-\mu_{12}\mu_{23}\mu_{24}}{2m_1m_2m_3m_4} \int \frac{d^3l}{(2\pi)^3} \frac{l^i}{[\mathbf{l}^2 + c_1 - i\epsilon][\mathbf{l}^2 - 2\frac{\mu_{23}}{m_3}\mathbf{l} \cdot \mathbf{q} + c_2 - i\epsilon][\mathbf{l}^2 - 2\frac{\mu_{24}}{m_4}\mathbf{l} \cdot \mathbf{q}_1 + c_3 - i\epsilon]} \\ \equiv q^i J_1^{(1c)} + q_\perp^i J_2^{(1c)} \quad (\text{A8})$$

and

$$J^{(2)ij} = \frac{-\mu_{12}\mu_{23}\mu_{24}}{2m_1m_2m_3m_4} \int \frac{d^3l}{(2\pi)^3} \frac{l^i l^j}{[\mathbf{l}^2 + c_1 - i\epsilon][\mathbf{l}^2 - 2\frac{\mu_{23}}{m_3}\mathbf{l} \cdot \mathbf{q} + c_2 - i\epsilon][\mathbf{l}^2 - 2\frac{\mu_{24}}{m_4}\mathbf{l} \cdot \mathbf{q}_1 + c_3 - i\epsilon]} \\ \equiv \left(\delta^{ij} - \frac{q^i q^j}{\mathbf{q}^2} - \frac{q_\perp^i q_\perp^j}{\mathbf{q}_\perp^2} \right) J_0^{(2c)} + \frac{q^i q^j}{\mathbf{q}^2} J_1^{(2c)} + \frac{q_\perp^i q_\perp^j}{\mathbf{q}_\perp^2} J_2^{(2c)} + \frac{q^i q_\perp^j + q_\perp^i q^j}{|\mathbf{q}||\mathbf{q}_\perp|} J_3^{(2c)}, \quad (\text{A9})$$

where the scalar integrals $J_m^{(r)}$ can easily be disentangled and have to be evaluated numerically. The corresponding expressions for topology II can be obtained by changing the denominators accordingly.

3. Amplitudes

Tables III and IV list the relevant amplitudes for this calculation. We only give the dominant amplitudes, i.e., the ones that contribute to the part proportional to $\epsilon(\Upsilon') \cdot \epsilon(\Upsilon)$ as was explained in the main text. We further notice that all box diagrams are proportional to the overall factor $\epsilon^a(\Upsilon')\epsilon^b(\Upsilon)g_\pi^2 g_{J'HH}g_{JHH}/F_\pi^2$.

TABLE III. All loops contributing to topology (c1) in Fig. 1. The mesons are listed as $[M1, M2, M3, M4]$; P and V denote intermediate pseudoscalar and vector mesons, respectively. The different flavors are dropped for simplicity—the full amplitude contains the sum of all possible ones.

Intermediate mesons	Amplitude
$[P, P, P, V]$	$8q_1 \cdot q_2 J^{(2)ab}$
$[P, V, P, V]$	$-8q_1 \cdot q_2 J^{(2)ab}$
$[V, P, V, P]$	$4\delta^{ab} q_1^i (2q_2^j J^{(2)ij} + q \cdot q_2 J^{(1)i})$
$[P, V, V, V]$	$4\delta^{ab} (q_1^i q \cdot q_2 - q_2^i q \cdot q_1) J^{(1)i}$
$[V, P, V, V]$	$4\delta^{ab} q_1^i (2q_2^j J^{(2)ij} + q \cdot q_2 J^{(1)i})$
$[V, V, P, V]$	$4\delta^{ab} (q_1^i q \cdot q_2 - q_2^i q \cdot q_1) J^{(1)i}$
$[V, V, V, P]$	$8\delta^{ai} \delta^{bj} q_1 \cdot q_2 J^{(2)ij} \\ + 4\delta^{ab} q_1^i (2q_2^j J^{(2)ij} + q \cdot q_2 J^{(1)i})$
$[V, V, V, V]$	$4\delta^{ab} (4\delta^{ij} q_1 \cdot q_2 J^{(2)ij} - q_2^i q \cdot q_1 J^{(1)i} \\ + q_1^i (q \cdot q_2 J^{(1)i} - 4q_2^j J^{(2)ij}))$

Finally, we need to consider the different flavors of the intermediate bottom mesons. For topology (c1) with a pair of charged pions four possibilities exist: $[B^{(*)+}, B^{(*)-}, B^{(*)+}, B^{(*)0}]$, $[B^{(*)-}, B^{(*)+}, B^{(*)-}, \bar{B}^{(*)0}]$, $[B^{(*)0}, \bar{B}^{(*)0}, B^{(*)0}, B^{(*)+}]$, and $[\bar{B}^{(*)0}, B^{(*)0}, \bar{B}^{(*)0}, B^{(*)-}]$. For topology (d1) this reduces to just two: $[B^{(*)+}, B^{(*)-}, \bar{B}^{(*)0}, B^{(*)0}]$ and $[\bar{B}^{(*)0}, B^{(*)0}, B^{(*)+}, \bar{B}^{(*)-}]$. For the case of neutral pions the number of possible diagrams doubles—a factor 2 that is balanced by the factor $\sqrt{2}$ in the $SU(3)$ light-meson matrix.

TABLE IV. All loops contributing to topology (d1) in Fig. 1; see Table III for further notation.

Intermediate mesons	Amplitude
$[P, P, V, V]$	$8q_1 \cdot q_2 J^{(2)ab}$
$[P, V, P, V]$	$4\delta^{ab} (q_1 \cdot q_2 (2\delta^{ij} J^{(2)ij} + q_2^j J^{(1)i}) \\ - q_1^i (2q_2^j J^{(2)ij} + q_2^2 J^{(1)i})) \\ - 8\delta^{ai} \delta^{bj} q_1 \cdot q_2 J^{(2)ij}$
$[V, V, P, P]$	$4\delta^{ab} q_1^i (2q_2^j J^{(2)ij} + q \cdot q_2 J^{(1)i})$
$[V, P, V, P]$	$4\delta^{ab} q_1^i ((q \cdot q_2 + 2q_1 \cdot q_2) J^{(1)i} - 2q_2^j J^{(2)ij})$
$[P, V, V, V]$	$-4\delta^{ab} (2q_1^i q_2^j J^{(2)ij} + q_2^i (q_1 \cdot q_2 - q_1^2) J^{(1)i})$
$[V, P, V, V]$	$-4\delta^{ab} q_1^i (2q_2^j J^{(2)ij} - (q \cdot q_2 + 2q_1 \cdot q_2) J^{(1)i})$
$[V, V, P, V]$	$-4\delta^{ab} (2q_1^i q_2^j J^{(2)ij} + q_2^i (q_1 \cdot q_2 - q_1^2) J^{(1)i})$
$[V, V, V, P]$	$-4\delta^{ab} q_1^i (2q_2^j J^{(2)ij} + (q_2^2 - q_1 \cdot q_2) J^{(1)i})$
$[V, V, V, V]$	$4\delta^{ab} (4\delta^{ij} q_1 \cdot q_2 J^{(2)ij} - q_2^i q \cdot q_1 J^{(1)i} \\ + q_1^i (q \cdot q_2 J^{(1)i} - 4q_2^j J^{(2)ij}))$

- [1] M. B. Voloshin and V. I. Zakharov, *Phys. Rev. Lett.* **45**, 688 (1980).
- [2] V. A. Novikov and M. A. Shifman, *Z. Phys. C* **8**, 43 (1981).
- [3] Y. P. Kuang and T. M. Yan, *Phys. Rev. D* **24**, 2874 (1981).
- [4] Y. P. Kuang, *Front. Phys. China* **1**, 19 (2006).
- [5] E. Eichten, S. Godfrey, H. Mahlke, and J. L. Rosner, *Rev. Mod. Phys.* **80**, 1161 (2008).
- [6] F.-K. Guo, P.-N. Shen, H.-C. Chiang, and R.-G. Ping, *Nucl. Phys.* **A761**, 269 (2005).
- [7] F.-K. Guo, P.-N. Shen, H.-C. Chiang, and R.-G. Ping, *Phys. Lett. B* **658**, 27 (2007).
- [8] Y.-H. Chen, J. T. Daub, F.-K. Guo, B. Kubis, U.-G. Meißner, and B.-S. Zou, *Phys. Rev. D* **93**, 034030 (2016).
- [9] I. Adachi (Belle Collaboration), [arXiv:1105.4583](https://arxiv.org/abs/1105.4583).
- [10] A. Bondar *et al.* (Belle Collaboration), *Phys. Rev. Lett.* **108**, 122001 (2012).
- [11] M. B. Voloshin, *Pis'ma Zh. Eksp. Teor. Fiz.* **37**, 58 (1983) [*JETP Lett.* **37**, 69 (1983)].
- [12] V. V. Anisovich, D. V. Bugg, A. V. Sarantsev, and B.-S. Zou, *Phys. Rev. D* **51**, R4619 (1995).
- [13] A. E. Bondar, R. V. Mizuk, and M. B. Voloshin, [arXiv:1610.01102](https://arxiv.org/abs/1610.01102).
- [14] F.-K. Guo, C. Hanhart, and U.-G. Meißner, *Phys. Rev. Lett.* **103**, 082003 (2009); F.-K. Guo, C. Hanhart, and U.-G. Meißner, *Phys. Rev. Lett.* **104**, 109901(E) (2010).
- [15] F.-K. Guo, C. Hanhart, G. Li, U.-G. Meißner, and Q. Zhao, *Phys. Rev. D* **83**, 034013 (2011).
- [16] M. Cleven, Q. Wang, F.-K. Guo, C. Hanhart, U.-G. Meißner, and Q. Zhao, *Phys. Rev. D* **87**, 074006 (2013).
- [17] T. Mannel and R. Urech, *Z. Phys. C* **73**, 541 (1997).
- [18] M. Cleven, F.-K. Guo, C. Hanhart, and U.-G. Meißner, *Eur. Phys. J. A* **47**, 120 (2011).
- [19] S. Fleming and T. Mehen, *Phys. Rev. D* **78**, 094019 (2008).
- [20] G. Burdman and J. F. Donoghue, *Phys. Lett. B* **280**, 287 (1992).
- [21] M. B. Wise, *Phys. Rev. D* **45**, R2188 (1992).
- [22] T. M. Yan, H. Y. Cheng, C. Y. Cheung, G. L. Lin, Y. C. Lin, and H. L. Yu, *Phys. Rev. D* **46**, 1148 (1992); T. M. Yan, H. Y. Cheng, C. Y. Cheung, G. L. Lin, Y. C. Lin, and H. L. Yu, *Phys. Rev. D* **55**, 5851(E) (1997).
- [23] R. Casalbuoni, A. Deandrea, N. Di Bartolomeo, R. Gatto, F. Feruglio, and G. Nardulli, *Phys. Rep.* **281**, 145 (1997).
- [24] F. Bernardoni, J. Bulava, M. Donnellan, and R. Sommer (ALPHA Collaboration), *Phys. Lett. B* **740**, 278 (2015).
- [25] I. W. Stewart, *Nucl. Phys.* **B529**, 62 (1998).
- [26] J. Hu and T. Mehen, *Phys. Rev. D* **73**, 054003 (2006).
- [27] T. Mehen and J. W. Powell, *Phys. Rev. D* **88**, 034017 (2013).
- [28] R. García-Martín and B. Moussallam, *Eur. Phys. J. C* **70**, 155 (2010).
- [29] B. Kubis and J. Plenler, *Eur. Phys. J. C* **75**, 283 (2015).
- [30] Z.-H. Guo and J. A. Oller, *Phys. Rev. D* **84**, 034005 (2011).
- [31] X.-W. Kang, B. Kubis, C. Hanhart, and U.-G. Meißner, *Phys. Rev. D* **89**, 053015 (2014).
- [32] K. M. Watson, *Phys. Rev.* **88**, 1163 (1952).
- [33] K. M. Watson, *Phys. Rev.* **95**, 228 (1954).
- [34] R. Omnès, *Nuovo Cimento* **8**, 316 (1958).
- [35] A. V. Anisovich and H. Leutwyler, *Phys. Lett. B* **375**, 335 (1996).
- [36] R. García-Martín, R. Kamiński, J. R. Peláez, J. Ruiz de Elvira, and F. J. Ynduráin, *Phys. Rev. D* **83**, 074004 (2011).
- [37] I. Caprini, G. Colangelo, and H. Leutwyler, *Eur. Phys. J. C* **72**, 1860 (2012).
- [38] P. Büttiker, S. Descotes-Genon, and B. Moussallam, *Eur. Phys. J. C* **33**, 409 (2004).
- [39] C. Patrignani *et al.* (Particle Data Group Collaboration), *Chin. Phys. C* **40**, 100001 (2016).
- [40] B. Moussallam, *Eur. Phys. J. C* **14**, 111 (2000).
- [41] J. F. Donoghue, J. Gasser, and H. Leutwyler, *Nucl. Phys.* **B343**, 341 (1990).
- [42] M. Hoferichter, C. Ditsche, B. Kubis, and U.-G. Meißner, *J. High Energy Phys.* **06** (2012) 063.
- [43] J. T. Daub, C. Hanhart, and B. Kubis, *J. High Energy Phys.* **02** (2016) 009.
- [44] B. Aubert *et al.* (BABAR Collaboration), *Phys. Rev. Lett.* **96**, 232001 (2006).
- [45] A. Sokolov *et al.* (Belle Collaboration), *Phys. Rev. D* **79**, 051103 (2009).
- [46] F.-K. Guo, C. Hanhart, Yu. S. Kalashnikova, P. Matuschek, R. V. Mizuk, A. V. Nefediev, Q. Wang, and J.-L. Winyen, *Phys. Rev. D* **93**, 074031 (2016).
- [47] H. Y. Zhou and Y. P. Kuang, *Phys. Rev. D* **44**, 756 (1991).
- [48] C. Meng and K.-T. Zhao, *Phys. Rev. D* **77**, 074003 (2008).
- [49] D.-Y. Chen, X. Liu, and X.-Q. Li, *Eur. Phys. J. C* **71**, 1808 (2011).
- [50] K. Abe *et al.* (Belle Collaboration), [arXiv:hep-ex/0512034](https://arxiv.org/abs/hep-ex/0512034).
- [51] Y. S. Surovtsev, P. Bydžovský, T. Gutsche, R. Kamiński, V. E. Lyubovitskij, and M. Nagy, *Phys. Rev. D* **92**, 036002 (2015).